Fretting-fatigue analysis of shot-peened aluminium and titanium test specimens

FRETTING-FATIGUE ANALYSIS OF SHOT-PEENED ALUMINIUM AND TITANIUM TEST SPECIMENS

Sabrina Vantadori, Andrea Zanichelli

Department of Engineering & Architecture, University of Parma

Parco Area delle Scienze 181/A, 43124 Parma, Italy

ABSTRACT

In last decades, many alleviation measures were proposed in order to improve the life of fretting fatigue affected components. In such a context, the shot peening treatment is worth noting. Therefore, in the present paper, the fatigue life of shot-peened aluminium and titanium alloy specimens, subject to fretting fatigue under partial slip regime, is assessed by means of the Carpinteri et al. criterion for fretting fatigue. Firstly, according to the superposition principle, the relaxed residual stresses (due to the shot peening treatment) are combined with the stress components due to fretting fatigue loading. Then fretting fatigue assessment is performed. In such a context, a novel theoretical law for the relaxed residual stress field is here proposed, the implementation of which shows very promising results in terms of fretting fatigue life estimation of the shot-peened specimens examined.

KEYWORDS

Al7050-T7451 alloy, fretting fatigue, relaxed residual stress, shot peening, Ti6Al4V alloy.

1. INTRODUCTION

Many in-service engineering components are subjected to vibrations. When such components are clamped against a different mechanical part, relative micro-displacements arise at contact surface that is, no nominal displacements are attained between them[1,2]. This contact phenomenon is named fretting or fretting wear[2].

Two different regimes can be distinguished on the basis of the magnitude of the relative displacement between the components in contact. In the case of global relative motion between the components, with micro-displacements generally of the order of 20-300 microns, the contact problem is characterised by a *gross slip regime*. In such a condition, both components oscillate relative to one another and the main damage phenomenon is the material wear[3-6]. On the other hand, when the relative micro-displacements are of the order of few microns, together with a magnitude of the load clamping the components sufficiently high to prevent complete sliding between them, the contact problem is characterised by a *partial slip regime*. Under such a regime, the contact surface consists of an inner stick region, with no relative displacements, and an outer slip region. The main damage phenomenon is the nucleation of cracks at the contact surface[4,7].

A remote fatigue loading, acting at least on one of the components under contact, is able to promote the evolution of surface damage.

It can lead to fatigue failure. This situation is referred to as *fretting fatigue*, which is well known to be different from plain fatigue, mainly due to the high stress level that characterises the region near the contact surface[3,8-10].

Fretting fatigue is recognised as a primary failure mode across a wide range of mechanical systems, such as dovetail joints[11-12], bolt and riveted joints[13-15], clamped joints[16], bearings[17], metallic cables[18-20], turbine components[21].

Many attempts were made in order to carry out possible alleviation measures, in order to improve the fatigue life of fretting affected components[22-33]. The majority of such palliatives were developed with the aim to counteract the high stress gradients that arise in the zone near the contact surface. In such a context it may be cited: surface coatings and lubrication to reduce the friction coefficient, thermomechanical treatments to improve tribological surface properties, shot and laser peening to induce near the surface both compressive residual stresses and microstructural plastic distortion, among others.

It is well known that shot peening significantly improves the fretting fatigue behaviour of treated components[23,34-36]. In particular, such treatment is mainly applied to engineering components characterised by either complex geometry (that is cross-sectional variations, chamfers, notches, hole edges), welding joints or heat-affected zones. Springs, connecting rods, gear wheels, shafts, axles and turbine blades are examples of typical shot-peened components.

Shot peening is a cold process consisting in hitting the surface to be treated with a jet of well-defined shots, at speeds generally between 20 and 120 m/s. The effects of shots impact are: (i) superficial plastic deformations, and (ii) compressive residual stresses, both limited to a material layer of the order of 0.1÷0.5 mm, without affecting the material inner part. Such effects are responsible for the improvement of fretting fatigue behaviour of the component.

Many researchers have recently proposed methodologies in order to analyse the effect of shot peening on engineering components[37-39]. Some attempts have been made in the context of shot-peened components subject to fretting fatigue loading[40-44]. To the best knowledge of the authors, most of them have taken into account experimental measurements of residual stress field, whereas a simple theoretical profile of residual stress field has been proposed by Araújo et al.[45].

Nevertheless, it is important to highlight that the superficial compressive stress state is not a static state, but may evolve. Such a phenomenon, known as *residual stress relaxation*[35,46], is considered as one of the main drawbacks of shot peening, and despite of on-going research on shot peening, it continues to be a challenge. Residual stress relaxation is mainly linked to plastic deformation flow and may be due to thermal, quasi-static loading, or cyclic loading. The latter condition in the case of fretting fatigue is particularly complex to be theoretically analysed and makes the fatigue assessment quite difficult[40,41].

In the present paper, fretting fatigue tests carried out on shot-peened aluminium and titanium alloys[40,47] are simulated by employing the multiaxial Carpinteri et al. criterion for fretting fatigue[48,49]. The stress field, employed as input data for the above criterion, takes into account both shot peening relaxed residual stresses and fretting fatigue stress field. In particular, a novel theoretical law for the relaxed residual stress field is here proposed, and its accuracy is verified by employing the experimental data reported in Ref. **[40]**. Based on the satisfactory results obtained in terms of estimated fatigue life, the same law is used to simulate the experimental campaign reported in Ref. **[47]**.

The present paper is structured as follows. In **Section 2** some basic concepts on shot peening treatment are provided. **Section 3** is devoted to the description of the input data, in terms of stress field, of the Carpinteri et al. criterion, and a novel theoretical law for the relaxed residual stress field is proposed. **Section 4** is dedicated to the description of the Carpinteri et al. criterion for fretting fatigue. The accuracy of the proposed theoretical law is verified in **Section 5**, by simulating the experimental campaign performed on aluminium alloy specimens[40]. Due to the satisfactory results obtained in terms of estimated fatigue life, in **Section 6** the same law is used to simulate an experimental campaign performed on titanium alloy specimens[47]. Finally, conclusions are summarised in **Section 7**.

2. SHOT PEENING TREATMENT: BASIC CONCEPTS

2.1 Treatment parameters

The effects produced by the shot peening treatment depend on several variables, related to both the mechanical and geometric properties of the treated engineering component and the parameters of the treatment itself. In last decades, such treatment was widely investigated and many enhancements in terms of parameters control were achieved[35,50].

More precisely, the treatment parameters are: material type and diameter of the shots, nozzle diameter and distance from the component, impact angle, shot velocity, peening time and surface coverage. Although such a large number of variables makes the definition of the process and its effects not straightforward, three main parameters are recognised, that is: surface coverage, shots type and peening intensity.

Relative to surface coverage, the ratio between the portion of the surface actually shot and the total area subject to the treatment is referred to as surface coverage. It depends on other process parameters and varies during the treatment, by increasing with peening time[51]. In particular, it is possible to identify the peening time value related to the complete coverage condition, and beyond which it is not possible to achieve any further improvements in terms of treatment effects on the component. Since nowadays complete coverage condition is generally attained in industrial applications, it is important to highlight that shot peening treatments may be considered to be ruled only by shots type and peening intensity.

Relative to shot type, the magnitude and depth of plastic deformations induced on the treated surface are strongly influenced by the type of shots, in terms of shape, sizes, material and hardness[34]. Uniformly sized spherical shots are usually employed and it is important to avoid their ovalization during the process. Therefore, the majority of peening is undertaken using metallic shots due to their good durability, even if glass and ceramic bleads are sometimes employed, especially for components made of aluminium, magnesium or titanium alloys.

Relative to peening intensity, measured in Almen, it is experimentally determined by measuring the deflection of a thin standard steel strip, which is fixed with four screws onto a metal block and then peened on one side only under the peening conditions to be analysed (more details related to Almen test strip may be found in Refs. **[52,53]**). Depending on the thickness of the steel strip used, the peening intensity is expressed in three different scale, that is Almen N, A and C, related to low, medium and high intensity, respectively. The peening intensity (or Almen intensity) may be considered the representative parameter of a shot peening treatment and it is used in practical applications to define the desired peening treatment of a given component[54].

2.2 Stability of residual stresses

As previously mentioned, residual stress relaxation may be due to thermal, quasi-static loading, or cyclic loading. Under cyclic

loading, such a relaxation generally takes place within three successive phases[46].

The first phase includes the initial loading and the successive inverse loading, constituting the quasi-static loading (first cycle). In such a phase the relaxation phenomenon is governed by both the quasi-static compressive yield strength and the Baushinger effect. Relaxation of residual stress is caused by the fact that the examined loading amplitude exceeds the quasi-static compressive yield strength of the material during the first cycle.

The second phase includes further cyclic loading, constituting the actual cyclic loading in the crack free phase. In such a phase the relaxation phenomenon is governed by the cyclic yield strengths. Relaxation of residual stress is caused by the fact that the examined loading amplitude exceeds the cyclic yield strengths of the material. Such a condition produces a cyclic work softening, that is a sudden increasing of plastic strain amplitude, and that occurs after a number of loading cycles to incubation during which the strain amplitude is constant, due to a quasi-elastic material behaviour. Note that, by increasing the loading amplitude, work softening becomes more pronounced and the number of loading cycles to incubation decreases.

The third phase includes further cyclic loading, constituting the crack growth phase. In such a phase the relaxation phenomenon becomes more pronounced, governed by the cyclic crack growth behaviour. The cause of relaxation is the same of that presented for the second phase, with a more pronounced work softening. The

changes of surface layer stress state, according to the three phases presented above, are mainly determined by loading type, amplitude and mean value of loading, initial amount of residual stress, and material state and its deformation behaviour. More precisely, four different behaviours may be distinguished:

(a) when neither quasi-static nor cyclic yield strengths are exceeded, residual stresses remain stable during both initial quasi-static loading and actual cyclic loading;

(b) when only quasi-static yield strength is exceeded, residual stresses significantly relax during the first cycle, but remain stable during actual cyclic loading;

(c) when only cyclic yield strengths are exceeded, residual stresses gradually relax during actual cyclic loading;

(d) when both quasi-static and cyclic yield strengths are exceeded, a pronounced residual stress relaxation due to the first cycle is followed by an additional gradual relaxation during actual cyclic loading.

3. STRESS INPUT DATA FOR THE CARPINTERI ET AL. CRITERION

The stress state represents one of input data for the Carpinteri et al. criterion for fretting fatigue (here used to estimate the lifetime of shot-peened specimens under fretting fatigue loadings). Such a stress state has to be computed by taking into account both the relaxed residual stress field, produced by both surface treatment and cyclic loading, and the stress produced by fretting fatigue

loading. Such two contributions may be independently evaluated and then combined according to the superposition principle, due to the fact that residual stresses affect the stress field acting on the mean value of some components of the stress tensor, as detailed in the following.

3.1 Shot peening relaxed residual stress: experimental observations

Residual stresses may be experimentally measured by means of the X-Ray Diffraction method or the Blind Hole Drilling method, the latter being a destructive test.

It is experimentally observed that shot peening produces residual stresses along both longitudinal and transversal direction, with comparable values, whereas the values of all the other stress components are negligible. More precisely, such residual stresses are compressive close to the surface, that is in the region characterised by plastic deformation, and generally become tensile with increasing depth. The inner tensile stresses arise in order to balance the superficial compressive layer. It is worth noting that the magnitude of such tensile stresses is negligible with respect to that of the superficial compressive ones.

A typical profile of relaxed residual stress induced by a shot peening treatment, and representing the stress distribution both along the longitudinal and transversal direction, σ^{res}, is shown in **Figure 1(a)**.

Figure 1.

In particular, the value of residual stress in correspondence of the material surface is always compressive: its value depends on many variables related to both the shot-peened component and the treatment parameters and tends to zero by increasing the number of loading cycles.

The depth of the compressive stress field, D_c, is of the order of a few hundred microns, and it is experimentally observed to be mainly linked to the Almen intensity of superficial treatment[51,55]. Moreover, such a field reaches its maximum value at a depth approximately equal to 1/4 of D_c depth[57], with an absolute value generally equal to about 2/3 of the material tensile yield strength, σ_y[45,56].

3.2 Shot peening relaxed residual stress: the theoretical law proposed

A theoretical law to evaluate the relaxed residual stress profile due to shot peening is here proposed.

More precisely, the experimental stress profile shown in **Figure 1(a)** is idealised by means of a bilinear curve, defined as follows (**Figure 1(b)**):

(1) the value of residual stress at the material surface is conservatively assumed equal to zero;

(2) by moving from the surface towards the inner part of the material, the residual stress field follows a linear behaviour until its maximum value is reached at a depth equal to $0.28D$, according to the assumption reported in Ref. **[57]**;

(3) the maximum value of the compressive residual stress is assumed to be equal to $2/3\,\sigma_y$ (absolute value), in accordance with the experimental observations previously mentioned[45,56];

(4) by moving from a depth of $0.28D$ towards the inner part of the material, the residual stress field follows a linear behaviour up to a depth, D_c, where the residual stress is equal to zero. Such a depth may be assumed to be related to the Almen intensity[51,55], by means of the linear correlation proposed by Kirk[58];

(5) by moving from D_c towards the inner part of the material, the residual stress field is assumed equal to zero, due to the fact that the values of the tensile stresses are negligible with respect to the compressive ones.

3.3 Fretting fatigue stress field

Let us consider a typical fretting fatigue configuration (**Figure 2**), in which two fretting pads, which may be characterised by either spherical or cylindrical shape, are pushed against a dog-bone specimen in partial slip regime. The reference frame, $OXYZ$, shown in **Figure 2** is also introduced.

A constant normal force, P, and a cyclic tangential force, $Q(t)$, are applied to the pads, whereas the specimen experiences a cyclic

axial stress, named bulk stress in the following, $\sigma_B(t)$, which is in-phase with $Q(t)$.

Figure 2.

In such a condition, the stress field in the vicinity of the contact zone can be evaluated by means of the analytical solutions available in the literature[59,60]. Only the stress field in the case of cylindrical pads is presented in the following: nevertheless, the stress field in the case of spherical pads may be deduced in a similar way[59].

According to the Hertzian theory, the contact semi-width, a, between two cylindrical half spaces, characterised by a curvature radius equal to R and experiencing a normal load P, is given by:

$$a = \sqrt{\frac{4PR}{\pi E^*}} \qquad \textbf{(1)}$$

being E^* the Young modulus for plane strain conditions.

In such a condition, a Hertzian *contact pressure distribution*, $p(x)$ (produced by the load P), arises between each pad and the specimen. In the vicinity of the contact zone, the stress field in the specimen is given by:

$$\sigma_x^P = -\frac{p_0}{a}\left[m\left(1+\frac{z^2+n^2}{m^2+n^2}\right) - 2z \right] \qquad \textbf{(2a)}$$

$$\sigma_z^P = -\frac{p_0}{a} m\left(1-\frac{z^2+n^2}{m^2+n^2}\right) \qquad \textbf{(2b)}$$

$$\tau_{xz}^{P}=\begin{cases}-\dfrac{p_0}{a}n\left(\dfrac{m^2-z^2}{m^2+n^2}\right) & \text{for } x\geq 0\\ \dfrac{p_0}{a}n\left(\dfrac{m^2-z^2}{m^2+n^2}\right) & \text{for } x<0\end{cases} \tag{2c}$$

where the functions m and n are given by:

$$m^2=\frac{1}{2}\left[\sqrt{\left(a^2-x^2+z^2\right)^2+4x^2z^2}+\left(a^2-x^2+z^2\right)\right] \tag{3a}$$

$$n^2=\frac{1}{2}\left[\sqrt{\left(a^2-x^2+z^2\right)^2+4x^2z^2}-\left(a^2-x^2+z^2\right)\right] \tag{3b}$$

p_0 being the maximum value of the contact pressure distribution:

$$p_0=\frac{2P}{\pi a} \tag{4}$$

On the other hand, the cyclic tangential force gives rise to a *contact shear distribution*, $q(x)$, between the pads and the specimen. In particular, a central inner stick domain (with a semi-width equal to c) and two lateral slip zones may be identified. According to Hills and Nowell[60], the presence of $\sigma_B(t)$ has to be taken into account by means of an eccentricity, e, of the stick zone. At the time instant for which $Q(t)$ attains its maximum value, the value of c and e can be computed by means of the following expressions:

$$c=a\sqrt{1-\frac{Q_a}{\mu P}} \tag{5a}$$

$$e=a\frac{\sigma_{B,a}}{4\mu p_0} \tag{5b}$$

Q_a and $\sigma_{B,a}$ being the amplitudes of the tangential force and the bulk stress, respectively, and μ the coefficient of friction.

The stress components in the specimen, when the cyclic tangential force attains its maximum value, are given by:

$$\sigma_x^Q = \begin{cases} \dfrac{\mu p_0}{a}\left\{\left[n\left(2-\dfrac{z^2-m^2}{m^2+n^2}\right)-2x\right]-\left[n_e\left(2-\dfrac{z^2-m_e^2}{m_e^2+n_e^2}\right)-2|x-e|\right]\right\} & \text{for } x \geq 0 \\ \dfrac{\mu p_0}{a}\left\{-\left[n\left(2-\dfrac{z^2-m^2}{m^2+n^2}\right)+2x\right]+\left[n_e\left(2-\dfrac{z^2-m_e^2}{m_e^2+n_e^2}\right)-2|x-e|\right]\right\} & \text{for } x < 0 \end{cases} \quad \textbf{(6a)}$$

$$\sigma_z^Q = \begin{cases} \dfrac{\mu\, p_0}{a}\left[-n\left(\dfrac{m^2-z^2}{m^2+n^2}\right)+n_e\left(\dfrac{m_e^2-z^2}{m_e^2+n_e^2}\right)\right] & \text{for } x \geq 0 \\ \dfrac{\mu\, p_0}{a}\left[n\left(\dfrac{m^2-z^2}{m^2+n^2}\right)-n_e\left(\dfrac{m_e^2-z^2}{m_e^2+n_e^2}\right)\right] & \text{for } x < 0 \end{cases} \quad \textbf{(6b)}$$

$$\tau_{xz}^Q = \frac{\mu\, p_0}{a}\left\{-\left[m\left(1+\frac{z^2+n^2}{m^2+n^2}\right)-2z\right]+\left[m_e\left(1+\frac{z^2+n_e^2}{m_e^2+n_e^2}\right)-2z\right]\right\} \quad \textbf{(6c)}$$

where the functions m_e and n_e are given by:

$$m_e^2 = \frac{1}{2}\left\{\sqrt{\left[c^2-(x-e)^2+z^2\right]^2+4(x-e)^2z^2}+\left[c^2-(x-e)^2+z^2\right]\right\} \quad \textbf{(7a)}$$

$$n_e^2 = \frac{1}{2}\left\{\sqrt{\left[c^2-(x-e)^2+z^2\right]^2+4(x-e)^2z^2}-\left[c^2-(x-e)^2+z^2\right]\right\} \quad \textbf{(7b)}$$

Figure 3 shows the stress component profiles due to fretting loading in correspondence of the longitudinal middle cross section of the specimen (that is XZ plane), at the trailing edge of the contact zone (that is $x=a$), due to $p(x)$ (**Figure 3(a)**) and $q(x)$ (**Figure 3(b)**).

Figure 3.

Moreover, the *cyclic bulk stress* only produces a normal stress component. In particular, the expression of such a stress component,

at the time instant for which both $Q(t)$ and $\sigma_B(t)$ attain their maximum values, is given by:

$$\sigma_x^B = \sigma_{B,m} + \sigma_{B,a} \tag{8}$$

where $\sigma_{B,m}$ is the mean value of $\sigma_B(t)$.

Finally, by superimposing the above stress contributions (see Eqs. (2), (6) and (8)), it is possible to evaluate the specimen stress tensor due to fretting fatigue loading. In particular, at the time instant in correspondence to the maximum value of both bulk stress and tangential force, the stress components turn out to be:

$$\sigma_x = \sigma_x^P + \sigma_x^Q + \sigma_x^B \tag{9a}$$

$$\sigma_z = \sigma_z^P + \sigma_z^Q \tag{9b}$$

$$\tau_{xz} = \tau_{xz}^P + \tau_{xz}^Q \tag{9c}$$

It is important to highlight that $\sigma_y = \nu(\sigma_x + \sigma_z)$ due to plane strain condition.

4. FRETTING FATIGUE LIFE ASSESSMENT: THE CARPINTERI ET AL. CRITERION

The fatigue life of shot-peened components subject to fretting fatigue loading is evaluated by means of the Carpinteri et al. criterion for fretting fatigue[48,49], that is a multiaxial criterion based on the concept of critical plane.

Firstly, the stress field is determined by considering both the relaxed residual stress (that is σ^{res} presented in **Section 3.2**), the

stress components due to fretting fatigue loading (Eqs. (9) presented in **Section 3.3**), and a loading ratio equal to -1.0.

The Critical Direction Method (CDM) proposed by Araújo et al.[61] is implemented in the criterion in order to determine the orientation of the critical plane.

The point on the above plane where to perform the fatigue life assessment (named verification point) needs to be identified, as detailed in the following. More precisely, such a point is assumed to be located on the critical plane, at a distance equal to $2d$ measured from the trailing edge, where d is the averaged grain size of the material, according to the critical distance defined by Taylor.

Subsequently, the amplitude, N_a, and the mean value, N_m, of the normal stress related to the critical plane, and the amplitude, C_a, of the shear stress lying on the critical plane are computed at the above verification point. According to the Carpinteri et al. criterion for fretting fatigue, a like-Goodman equation is used to compute an equivalent normal stress amplitude, $N_{eq,a}$:

$$N_{eq,a} = N_a + \sigma_{af-1}\left(\frac{N_m}{\sigma_u}\right) \quad \textbf{(10)}$$

where σ_u is the ultimate tensile strength of the material, and σ_{af-1} is the material fatigue strength under fully reversed normal stress at N_0 loading cycles.

Note that Eq. (10) takes into account the strength decrease due to the simultaneous presence of a tensile mean normal stress and an

alternating normal stress. Therefore, N_m should be conservatively assumed to be equal to zero when N_m is a compressive stress. Nevertheless, according to Stephens et al.[62], the Goodman relation can be extrapolated for negative mean stress, if the stress level is beneath the yielding of the material. Therefore, in order to take into account the beneficial effect produced by the compressive residual stress field on fatigue life, N_m is considered in the computation of $N_{eq,a}$ even in the case of negative value.

Finally, according to the criterion, the fatigue life is evaluated by means of an iterative procedure. More precisely, the number of loading cycles to failure, N_{cal}, is computed by solving the following expression:

$$\sqrt{N_{eq,a}^2+\left(\frac{\sigma_{af,-1}}{\tau_{af,-1}}\right)^2\left(\frac{N_{cal}}{N_0}\right)^{-\frac{2}{m}}\left(\frac{N_0}{N_{cal}}\right)^{-\frac{2}{m^*}}C_a^2}=\sigma_{af,-1}\left(\frac{N_{cal}}{N_0}\right)^{-\frac{1}{m}} \quad \textbf{(11)}$$

where $\sigma_{af,-1}$ and $\tau_{af,-1}$ are the material fatigue strength at a reference number of loading cycles, N_0, under fully reversed normal loading and shear loading, respectively, whereas m and m^* are the slope of the S-N curve under fully reversed normal loading and shear loading, respectively.

5. SHOT-PEENED SPECIMENS UNDER SPHERICAL CONTACT

The accuracy of the Carpinteri et al. criterion is verified by the simulation of an experimental campaign carried out on shot-peened

specimens, made of Al7075-T651 alloy, and experiencing a spherical contact[40].

5.1 Experimental campaign description

Thirteen flat dog-bone test specimens, made of Al7075-T651 alloy, were machined. The mechanical and fatigue properties of the material are listed in **Table 1**[40], whereas the averaged grain size is equal to 50 μm[49].

Table 1.

Before testing, seven specimens (from No. T1 to T7) were subjected to a shot peening treatment, according to AMS-2430 standard[63], whereas six specimens (from No. R1 to R6) were directly tested without any treatment.

The superficial treatment was characterised by an Almen intensity equal to 20-24A and a complete coverage condition, which corresponds to a deflection in the Almen test strip equal to 500-600 μm[64]. In more detail, steel balls with a diameter equal to 600 μm and a hardness of 45-52 HRC were used. After shot peening, the specimens were polished in order to restore the un-treated superficial roughness. The coefficient of friction after the polish treatment was equal to 1.18, similar to that of the as-received specimens equal to 1.20.

The residual stress field up to a depth of 1 mm was measured by means of the Blind-Hole method[65]. The residual stress distribution,

measured both immediately after the superficial treatment (that is, before fretting fatigue tests) and after 10^4 fretting fatigue loading cycles, is shown in **Figure 4**, where each band represents different values between the measurements performed[40]. It was proved that such distributions were quite independent to the stress level[40].

Figure 4.

A customized servo-hydraulic machine[40] was used to perform the fretting fatigue tests. In particular, the experimental tests were carried out in partial slip regime, by using two spherical pads ($R = 100$ mm) and by applying five different loading conditions[40]. The loading parameters and the corresponding experimental fretting fatigue life, N_{exp}, are listed in **Table 2** for specimens No. R1-R6 and in **Table 3** for specimens No. T1-T7.

Table 2.

Table 3.

5.2 Results and discussion

The criterion presented in **Section 4** is here applied to simulate the above experimental campaign.

More precisely, firstly a comparison between experimental and estimated fatigue life, $N_{cal,R}$, for each test of the R-series (that is as-received specimens) is shown in **Figure 5**. Note that, the dashed lines correspond to $N_{exp}/N_{cal,R}$ equal to 0.5 and 2, and defining the scatter band 2. Moreover, the values of both N_{exp} and $N_{cal,R}$, and the ratio $N_{cal,R}/N_{exp}$ are listed in **Table 2**.

Figure 5.

It can be observed that all results fall within the scatter band 2, and therefore the estimations seem to be quite satisfactory. The criterion provides conservative estimations for tests No. from R1 to R4, whereas for the loading configuration of tests No. R5 and R6 results $N_{cal,R} > N_{exp}$ (**Table 2**).

It is also possible to quantify the accuracy of the criterion by means of the root mean square error method[66,67], where such an error, T_{RMS}, is computed as:

$$T_{RMS} = 10^{E_{RMS}} \quad \text{with} \quad E_{RMS} = \sqrt{\frac{\sum_{i=1}^{n} \log^2\left(N_{exp}/N_{cal,R}\right)_i}{n_s}} \qquad \textbf{(12)}$$

being n_s the total number of specimens of the considered series.

As far as the R-series is concerned, the value of T_{RMS} is equal to 1.50, that highlights a quite good accuracy of the criterion employed, since $T_{RMS} = 1$ represents a perfect correlation between experimental and estimated values.

A numerical simulation of the above experimental campaign was also provided by Vázquez et al.[41], by employing a numerical methodology that combines crack initiation and propagation. The comparison between experimental and estimated fatigue life is shown in **Figure 5**. It can be observed that almost all the results fall within the scatter band 2, and the computed value of T_{RMS} is equal to 1.59.

Then, the comparison is performed between experimental and estimated fatigue life for each test of the T-series (that is relaxed shot-peened specimens). Two relaxed residual stress field are alternatively taken into account in the calculation and more precisely:

(1) the experimental one measured after 10^4 loading cycles (see **Figure 4**). In such a case, the curve moving in the centre of the band shown in **Figure 4** is considered in the calculation;

(2) the theoretical one, described in **Section 3.2.** The main parameters of such a theoretical curve are: $\sigma_{\max}^{res} = -335\,\text{MPa}$, $D_{\max} = 140\,\mu\text{m}$ and $D_c = 500\,\mu\text{m}$, being D_c equal to about the Almen test strip deflection for aluminium alloys[58].

The number of loading cycles to failure, $N_{cal,T}^{(1)}$ and $N_{cal,T}^{(2)}$, for the case (1) and (2), respectively, are computed and the comparison with the experimental ones is shown in **Figure 6**. Moreover, the values of both N_{exp}, $N_{cal,T}^{(1)}$ and $N_{cal,T}^{(2)}$, and the ratios $N_{cal,T}^{(1)} \big/ N_{exp}$ and $N_{cal,T}^{(2)} \big/ N_{exp}$ are listed in **Table 3.**

Figure 6.

For the case (1), it can be observed that the estimations are in good agreement with the experimental fatigue lives, with all results into scatter band 2, and with a T_{RMS} value equal to 1.34.

Even for the case (2), it can be observed that the estimations are in good agreement with the experimental fatigue lives, with almost all results into scatter band 2, and a T_{RMS} value equal to 1.54.

A numerical simulation of such T-series specimens was also provided by Vázquez et al.[41]. The comparison between experimental and estimated fatigue life is shown in **Figure 6**, that highlights estimations generally non conservative, with a value of $T_{RMS} = 1.36$.

Therefore, it can be stated that the Carpinteri et al. criterion for fretting fatigue provides results characterised by a satisfactory accuracy, comparable with that related to more complex and time-consuming approaches, as that by Vázquez et al.[41].

Moreover, the proposed theoretical law for the relaxed residual stress seems to be a convenient solution to be adopted, especially when no experimental residual stress measurements are available.

6. SHOT PEENED SPECIMENS UNDER CYLINDRICAL CONTACT

The accuracy of the Carpinteri et al. criterion, implementing the theoretical law proposed for the relaxed residual stress, is verified by the simulation of an experimental campaign carried out on shot-

peened specimens, made of Ti6Al4V alloy, and experiencing a cylindrical contact[47].

6.1 Experimental campaign description

Eleven flat dog-bone test specimens, made of Ti6Al4V alloy, were machined by a wire electrical discharge machining method. All specimens were low stress ground to obtain a smooth surface finish. The mechanical and fatigue properties are listed in **Table 4**[45,47], whereas the averaged grain size is equal to 10 μm[47].

Table 4.

Before testing, all the specimens (from No. S1 to S11) were subjected to a shot peening treatment.

The superficial treatment was characterised by three different values of the Almen intensity equal to 4A (specimens from No. S1 to S4), 7A (specimens from No. S5 to S8), and 10A (specimens from No. S9 to S11). The surface coverage was kept at 100% for all specimens[47]. In more detail, all specimens were shot-peened as per SAE Aerospace Materials Specification (AMS) 2431 with standard cast steel balls with a diameter equal to 4300 μm. The coefficient of friction after the shot peening treatment was equal to 1.0[47].

A servo-hydraulic uniaxial test machine was used to perform the fretting tests. In particular, the experimental tests were carried out in partial slip regime, by using two cylindrical pads ($R = 50.4\,\text{mm}$) and the loading condition reported in **Table 5**[47]. The loading

parameters and the corresponding experimental fretting fatigue life, N_{exp}, are listed in the above Table for each tested specimen.

Table 5.

About loading conditions, two cylindrical pads were pressed against the specimen width surface with a constant contact force via lateral springs, which was monitored through a force transducer in each test. The applied axial force and shear (tangential) force on the specimen ware measured by monitoring the two force transducers, one on each side of the specimen[47].

6.2 Results and discussion

The criterion presented in **Section 4** is here applied to simulate the above experimental campaign.

A comparison is performed between experimental and estimated fatigue life for each test of the S-series. The relaxed residual stress fields taken into account in the calculation are assumed in accordance with the theoretical one, described in **Section 3.2.** The main parameters of such theoretical curves are:

(a) for the specimens from S1 to S4 (Almen intensity equal to 4A):

$\sigma_{\max}^{res} = -620\,\text{MPa}$, $D_{\max} = 32\,\mu\text{m}$ and $D_c = 113\,\mu\text{m}$;

(b) for the specimens from S5 to S8 (Almen intensity equal to 7A):

$\sigma_{\max}^{res} = -620\,\text{MPa}$, $D_{\max} = 37\,\mu\text{m}$ and $D_c = 135\,\mu\text{m}$;

(c) for the specimens from S9 to S11 (Almen intensity equal to 10A):

$\sigma_{\max}^{res} = -620\,\text{MPa}$, $D_{\max} = 70\,\mu\text{m}$ and $D_c = 248\,\mu\text{m}$;

being, for each of the above case, D_c equal to about 90% of the Almen test strip deflection for titanium alloys[58].

The number of loading cycles to failure, $N_{cal,S}$ is computed and the comparison with the experimental one is shown in **Figure 7**. Moreover, the values of both N_{exp} and $N_{cal,S}$, and the ratio $N_{cal,S}/N_{exp}$ are listed in **Table 5**.

Figure 7.

It can be observed that the estimations are in quite good agreement with the experimental values, by confirming that the theoretical curve proposed for the relaxed residual stress is a convenient solution. As a matter of fact, in general the results fall into scatter band 2, except that related to specimen No. S5 falling into scatter band 3, with a T_{RMS} value equal to 1.66.

7. CONCLUSIONS

In the present paper, the fatigue life of shot-peened aluminium and titanium alloy specimens, subject to fretting fatigue under partial slip regime, has been assessed by means of the Carpinteri et al. criterion for fretting fatigue.

In order to determine the actual stress field, a novel theoretical law for the relaxed residual stress field has been proposed.

Firstly, an experimental campaign performed on Al7075-T651 alloy specimens, experiencing fretting fatigue with a spherical contact, has been simulated. Then, the same theoretical law has been employed to simulate an experimental campaign, performed on Ti6Al4V alloy specimens, experiencing fretting fatigue with a cylindrical contact.

In more detail, the following values of the T_{RMS} have been computed:

- for the Al7075-T651 alloy shot-peened specimens: $T_{RMS} = 1.54$;
- for the Ti6Al4V alloy shot-peened specimens: $T_{RMS} = 1.66$;

Therefore, the proposed theoretical law seems to be a promising tool, especially in the case when the actual relaxed residual stress profile is not experimentally measured.

DECLARATION OF COMPETING INTEREST

The authors declare that they have no known competing financial interests or personal relationships that could have appeared to influence the work reported in this paper.

ACKNOWLEDGEMENTS

The authors gratefully acknowledge the financial support of the Italian Ministry of Education, University and Research (MIUR), Research Grant PRIN 2017 No. 2017HFPKZY on “Modelling of constitutive laws for traditional and innovative building materials”.

REFERENCES

[1] Waterhouse R.B. Fretting fatigue. *Int Mater Rev*. 1992; 37: 77-97.

[2] Nowell D. Recent developments in the understanding of fretting fatigue. *Proceeding of the 15th European Conference on Fracture (ECF-15)*, 2005.

[3] Endo K., Goto H. Initiation and propagation of fretting fatigue cracks. *Wear*, 1976; 38: 311-324.

[4] Berthier Y., Vincent L., Godet M. Fretting fatigue and fretting wear. *Tribol Int*, 1989; 22: 235-242.

[5] Blades L., Hills D., Nowell D., Evans K.E., Smith C. An exploration of debris types and their influence on wear rates in fretting. *Wear*, 2020; 450-451, 203252.

[6] Dreano A., Fouvry S., Guillonneau G. Understanding and formalization of the fretting-wear behavior of a cobalt-based alloy at high temperature. *Wear*, 2020; 452-453, 203297.

[7] Hurricks P.L. Mechanism of fretting. *Wear*, 1970; 15: 389-409.

[8] Szolwinski M.P., Farris T.N. Mechanics of fretting fatigue crack formation. *Int J Fatigue*, 1997; 19: 39-49.

[9] Carpinteri A., Vantadori S., Zanichelli A. Lifetime estimation of mechanical assemblies under constant amplitude fretting fatigue loading. *Fatigue Fract Eng Mater Struct*, 2019; 42: 1927-1936.

[10] Han Q.N., Rui S.S., Qiu W., Su Y., Ma X., He Z., Cui H., Zhang H., Shi H.J. Subsurface crack formation and propagation of fretting fatigue in Ni-based single-crystal superalloys. *Fatigue Fract Eng Mater Struct*, 2019; 42, 11: 2520-2532.

[11] Chen J.J., Liu L., Li S.X., Yu S.R., He Y.N. Experimental and numerical investigation on crack initiation of fretting fatigue of dovetail. *Fatigue Fract Eng Mater Struct*, 2018; 41: 1426-1436.

[12] Minaii K., Farrahi G.H., Karimpour M., Bahai H., Majzoobi G.H. Investigation of microstructure effect on fretting fatigue crack initiation using crystal plasticity. *Fatigue Fract Eng Mater Struct*, 2019; 42: 640-650.

[13] Chung C.S., Kim H.K. Fatigue strength of self-piercing riveted joints in lap-shear specimens of aluminium and steel sheets. *Fatigue Fract Eng Mater Struct*, 2016; 39: 1105-1114.

[14] Juoksukangas J., Lehtovaara A., Mäntylä A. Experimental and numerical investigation of fretting fatigue behavior in bolted joints. *Tribol Int*, 2016; 103: 440-448.

[15] Moraes J.F.C., Rao1 H.M., Jordon J.B., Barkey M.E. High cycle fatigue mechanisms of aluminum self-piercing riveted joints. *Fatigue Fract Eng Mater Struct*, 2018; 41: 57-70.

[16] Michnej M., Guzowski S. Fretting wear simulation in a clamped joint based on the example of a rail vehicle wheel set. *Wear*, 2019; 438-439, 102654.

[17] Brinji O., Fallahnezhad K., Meehan P.A. Analytical model for predicting false brinelling in bearings. *Wear*, 2020; 444-445, 203135.

[18] Fadel A.A., Rosa D., Murça L.B., Fereira J.L.A., Araújo J.A. Effect of high mean tensile stress on the fretting fatigue life of an Ibis steel reinforced aluminium conductor. *Int J Fatigue*, 2012; 42: 24–34.

[19] Araújo J.A., Castro F.C., Pommier S.., Bellecave J, Meriaux J. On the design and test of equivalent configurations for notch and fretting fatigue. *Fatigue Fract Eng Mater Struct*, 2016; 39: 1241–1250.

[20] Erena D., Vázquez Valeo J., Navarro C., Domínguez J. New fatigue device for testing cables: Design and results. *Fatigue Fract Eng Mater Struct*, 2019; 42, 8: 1826-1837.

[21] Sharma A., Sadeghi F., Sharma A. Experimental investigation of fretting wear of coated spring clip and inlet ring in land-based gas turbines at elevated temperature. *Wear*, 2020; 446-447, 203200.

[22] Proudhon H., Fouvry S., Yantio G.R. Determination and prediction of the fretting crack initiation: introduction of the (P, Q, N) representation and definition of a variable process volume. *Int J Fatigue*, 2008; 28: 707-713.

[23] Vázquez J., Navarro C., Domínguez J. Analysis of the effect of a textured surface on fretting fatigue. *Wear*, 2013; 305, 1-2, 23-35.

[24] Li X., Yang J.W., Li M.H., Zuo Z. An investigation on fretting fatigue mechanism under complex cyclic loading conditions. *Int J Fatigue*, 2016; 88: 227-235.

[25] Ding H.H., Fridrici V., Guillonneau G., Sao-Joao S., Geringer J., Fontaine J., Kapsa P. Investigation on mechanical properties of tribofilm formed on Ti–6Al–4V surface sliding against a DLC coating by nano-indentation and micro-pillar compression techniques. *Wear*, 2019; 432-433, 202954.

[26] Kowalski S., Cygnar M. The application of TiSiN/TiAlN coatings in the mitigation of fretting wear in push fit joints. *Wear*, 2019; 426-427: 725-734.

[27] Ma L., Eom K., Geringe J., Jun, T.-S., Kim K. Literature review on fretting wear and contact mechanics of tribological coatings. *Coatings*, 2019; 9, 501.

[28] Amanov A. Improvement in mechanical properties and fretting wear of Inconel 718 superalloy by ultrasonic nanocrystal surface modification. *Wear*, 2020; 446-447, 203208.

[29] Dyson C.J., Chittenden R.J., Priest M., Fox M.F., Hopkins W.A. Representative Tribometer Testing of Wire Rope Fretting Contacts: The Effect of Lubrication on Fretting Wear. *Tribol Trans*, 2020; 63: 557-574.

[30] Erena D., Vázquez J., Navarro C., Domínguez J. Numerical analysis of toroidal voids as stress relievers in shrink-fitted shafts. *Trib Int*, 2020; 143, 105996.

[31] Song B., Murray J.W., Wellman R.G., Pala Z., Hussain T. Dry sliding wear behaviour of HVOF thermal sprayed WC-Co-Cr and WC-CrxCy-Ni coatings. *Wear*, 2020; 442-443, 203114.

[32] Sun Z., Xu C.-M., Peng Y.-X., Shi Y.-Y., Zhang Y.-W. Fretting tribological behaviors of steel wires under lubricating grease with compound additives of graphene and graphite. *Wear*, 2020; 454-455, 203333.

[33] Xu R., Qin H., Zhai W., Chen X., Lu W., Chang S. Comparative study on aromatic thermosetting co-polyester (ATSP) coating and nickel-aluminum bronze on under torsional fretting wear. *Wear*, 2020; 454-455, 203290.

[34] Kirk D. Shot peening. *Aircraft Eng Aerosp Tech*, 1999; 77, 4: 349-361.

[35] Wagner L. (Ed.). Shot Peening. Proceedings of the 8th International Conference on Shot Peening, Wiley–VCH, Weinheim, 2003.

[36] Liu X., Liu J., Zuo Z., Zhang H. Effects of shot peening on fretting fatigue crack initiation behaviour. *Materials*, 2019; 12, 743.

[37] Rama Krishna L., Madhavi Y., Sahithi T., Srinivasa Rao D., Ijeri V.S., Prakash O., Gaydos S.P. Enhancing the high cycle fatigue life of high strength aluminum alloys for aerospace applications. *Fatigue Fract Eng Mater Struct*, 2019; 42, 3: 698-709.

[38] Arakawa J., Hanaki T., Hayashi Y., Akebono H., Sugeta A. Evaluating the fatigue limit of metals having surface compressive residual stress and exhibiting shakedown. *Fatigue Fract Eng Mater Struct*, 2020; 43, 2: 211-220.

[39] Takahashi K., Kogishi Y., Shibuya N., Kumeno F. Effects of laser peening on the fatigue strength and defect tolerance of aluminum alloy. *Fatigue Fract Eng Mater Struct*, 2020; 43, 4: 845-856.

[40] Vázquez J., Navarro C., Domínguez J. Experimental results in fretting fatigue with shot and laser peened Al 7075-T651 specimens. *Int J Fatigue*, 2012; 40: 143–53.

[41] Vázquez J., Navarro C., Domínguez J. A model to predict fretting fatigue life including residual stresses. *Theor Appl Fract Mec*, 2014; 73: 144–51.

[42] Majzoobi G.H., Abbasi F. On the effect of shot-peening on fretting fatigue of Al7075-T6 under cyclic normal contact loading. *Surface and Coatings Technology*, 2017; 328: 292-303.

[43] Yang Q., Zhou W., Gai P., Zhang X., Fu X., Chen G., Li Z. Investigation on the fretting fatigue behaviors of Ti-6Al-4V dovetail joint specimens treated with shot-peening. *Wear*, 2017; 372-373: 81-90.

[44] Liu X., Liu J., Zuo Z., Zhang H. Effects of shot peening on fretting fatigue crack initiation behaviour. *Materials*, 2019; 12, 5, 743.

[45] Araújo J.A., Nowell D. Mixed high low fretting fatigue of Ti6Al4V: Test and modelling. *Trib Int*, 2009; 42: 1276–1285.

[46] Schulze V. Modern Mechanical Surface Treatment. Wiley-VCH, 2006.

[47] Sabelkin V., Martinez S.A., Mall S., Sathish S., Blodgett M.P., Effects of shot-peening intensity on fretting fatigue crack-initiation behaviour of Ti–6Al–4V. *Fatigue Fract Eng Mater Struct*, 2005; 28: 321–332.

[48] Vantadori S., Zanichelli A., Araújo J.A. Fretting fatigue of 7050-T7451 Al alloy: the influence of bulk mean stress. *Int J Fatigue*, 2020; 140, 105816.

[49] Vantadori S., Vázquez J., Zanichelli A. Fretting fatigue and shot peening: a multiaxial fatigue criterion including residual stress relaxation. *Trib Int*, 2020; 151, 106537.

[50] Chaudhary K. Importance of controlling parameters in shot peening process. *J Emerg Techn Innov Research*, 2017; 4: 220-223.

[51] Farrahi G.H., Lebrun J.L., Couratin D. Effect of shot peening on residual stress and fatigue life of a spring steel. *Fatigue Fract Eng Mater Struct*, 1995; 18, 2: 211-220.

[52] Shot peening, computer monitored. SAE Standard AMS 2432 D.

[53] Champaigne J. Shot peening intensity measurement. *The shot peener*, 1992; 6, 4, 1992082.

[54] Vielma A.T., Llaneza V., Belzunce F.J. Shot peening intensity optimization to increase the fatigue life of a quenched and tempered structural steel. *Proceedia Engineering*, 2014; 74: 273-278.

[55] Sabelkin V., Martinez S.A., Mall S., Sathish S., Blodgett M.P. Effects of shot-peening intensity on fretting fatigue crack-initiation behaviour of Ti–6Al–4V. *Fatigue Fract Engng Mater Struct*, 2005; 28: 321–332.

[56] Higounenc O., Correlation of shot peening parameters to surface characteristic. *Proceedings of the 9th International Conference on Shot Peening*, Paris, 2005; 2005047.

[57] Gao Y.K., Yao M., Li J.K. An Analysis of Residual Stress Fields Caused by Shot Peening. *Metallurgical Mat Trans A*, 2002; 33A, 1775.
[58] Kirk D. Estimate Compressed Layer Depth by Using Almen Peening Intensity. *The Shot Peener*, 2014; 28, 2: 30-38.
[59] Johnson K.L. Contact mechanics. Cambridge, UK: Cambridge University Press; 1985.
[60] Hills D.A., Nowell D. Mechanics of Fretting Fatigue. Springer Netherlands; 1994.
[61] Araújo J.A., Almeida G.M.J., Ferreira J.L.A., da Silva C.R.M., Castro F.C. Early cracking orientation under high stress gradient: the fretting. *Int J Fatigue*, 2017; 100: 302-311.
[62] Stephens R.I., Fatemi A., Stephens R.R., Fuchs H.O. Metal Fatigue in Engineering. Second edition, John Wiley & Sons; 2000.
[63] Shot peening, automatic. SAE Standard AMS 2430 R, AMS B Finishes Processes And Fluids Committee; 2009.
[64] Jain A. A database for shot peening parameters and desired residual stress distribution. *Proceedings of the International Conference on Shot Peening and Blast Cleaning*, Bhopal, 1996.
[65] Determining residual stresses by the Hole-Drilling Strain-Gage Method. ASTM Standard E 837.
[66] Vantadori S., Carpinteri A., Fortese G., Ronchei C., Scorza D., Zanichelli A. Fatigue lifetime evaluation of notched components: implementation of the control volume concept in a strain-based LCF criterion. *Theor Appl Fract Mech*, 2018; 97: 400–8.
[67] Vantadori S., Carpinteri A., Luciano R., Ronchei C., Scorza D., Zanichelli A. Mean stress effect on fatigue life estimation for Inconel 718 alloy. *Int J Fatigue*, 2020; 133: 105391.

NOMENCLATURE

a	theoretical Hertzian contact semi-width
c	semi-width of the contact stick zone
C_a	amplitude of the shear stress component lying on the critical plane
d	critical distance
D_c	depth of compressive stress field due to shot peening
$D_{\max}$	depth at which $\sigma^{res} = \sigma^{res}_{\max}$
e	eccentricity of the contact stick zone
E	Young modulus
$E*$	Young modulus for plane strain conditions
m	slope of the S-N curve under fully reversed normal stress
m^*	slope of the S-N curve under fully reversed shear stress
N_a	amplitude of the normal stress component acting on the critical plane
$N_{eq,a}$	equivalent normal stress amplitude
N_{cal}	calculated fretting fatigue life
N_{exp}	experimental fretting fatigue life
N_m	mean value of the normal stress component acting on the critical plane
p_0	maximum value of the theoretical Hertzian contact pressure distribution
$p(x)$	theoretical Hertzian contact pressure distribution
P	constant normal load
Q	cyclic tangential load
Q_a	amplitude of tangential load
$q(x)$	theoretical Hertzian contact shear distribution
R	pads radius

μ	friction coefficient
ν	Poisson's coefficient
$\sigma_{af,-1}$	material fatigue strength under fully reversed normal stress at N_0 loading cycles
σ_B	cyclic axial bulk stress
$\sigma_{B,a}$	amplitude of axial bulk stress
$\sigma_{B,m}$	mean value of axial bulk stress
σ^{res}	shot peening relaxed residual stress
$\sigma^{res}_{\max}$	maximum value of shot peening relaxed residual stress
σ_u	ultimate tensile strength
σ_y	yield strength
$\tau_{af,-1}$	material fatigue strength under fully reversed shear stress at N_0 loading cycles

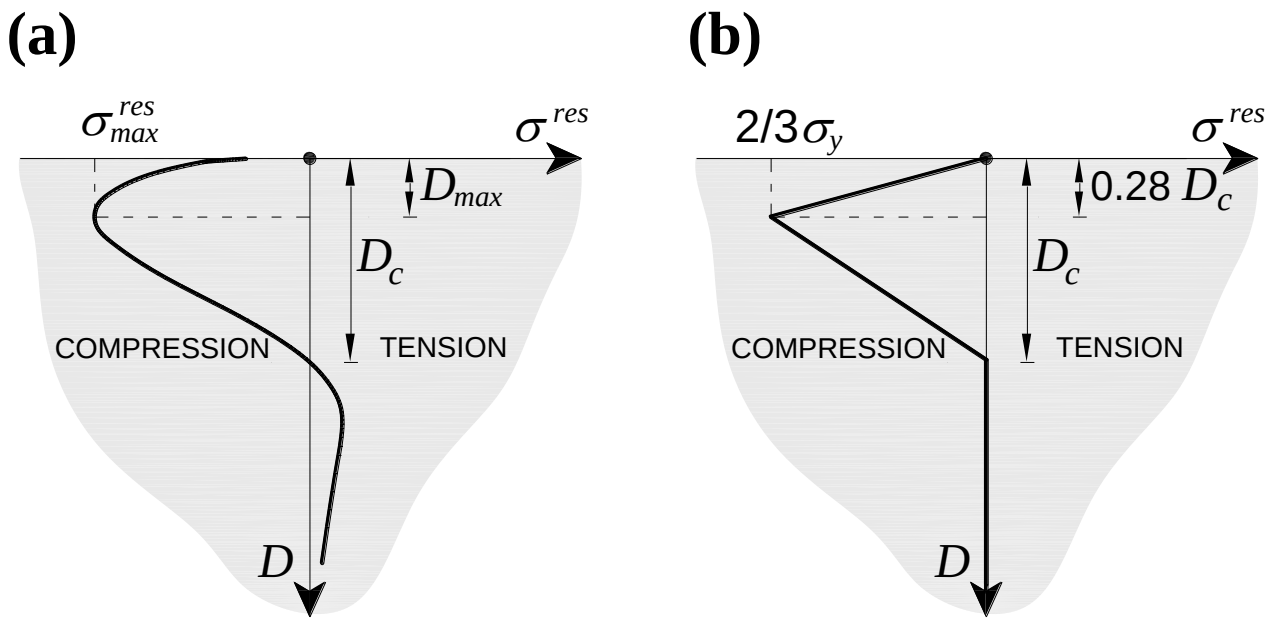

Figure 1. Relaxed residual stresses induced by shot peening: (a) typical experimental profile; (b) idealised bilinear profile.

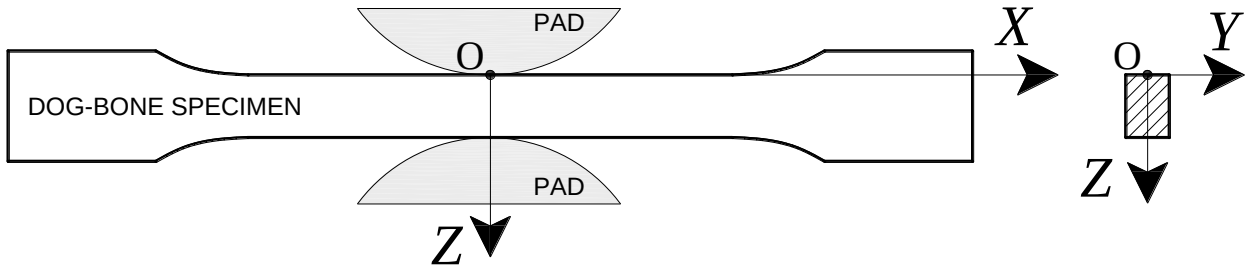

Figure 2. Typical fretting fatigue test configuration.

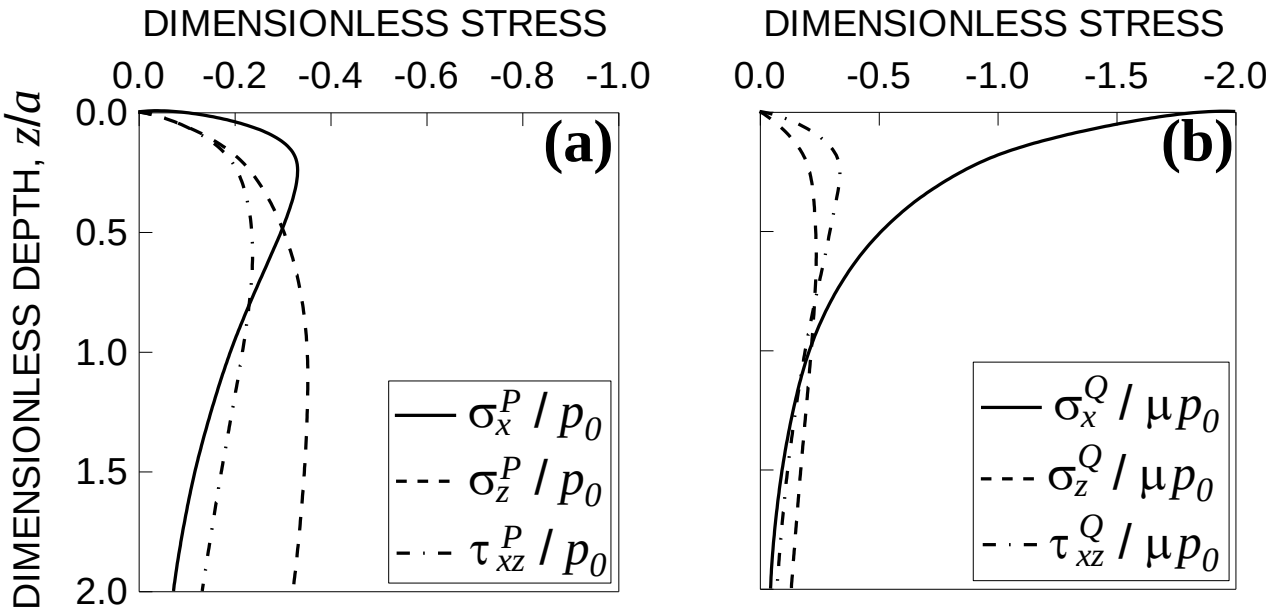

Figure 3. Stress component profiles at the trailing edge, due to fretting loading under partial slip regime: (a) normal load, P, and (b) tangential load, Q.

Table 1. Mechanical and fatigue properties of Al7075-T651 alloy[40].

MATERIAL	E [GPa]	ν	σ_y [MPa]	σ_u [MPa]	$\sigma_{af,-1}$ [MPa]	m	$\tau_{af,-1}$ [MPa]	m^*	N_0 [cycles]
Al7050-T651	71	0.33	503	572	193	8.20	111	8.20	$2\ 10^6$

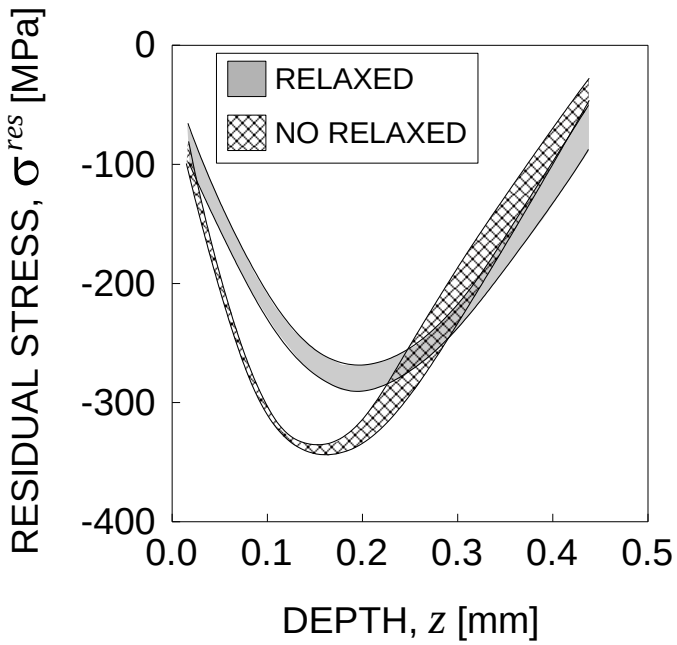

Figure 4. Measured residual stress profile due to shot peening treatment performed on specimens No. T1-T7.

Table 2. Loading parameters, experimental and estimated fretting fatigue life for specimens No. R1-R6.

TEST No.	P [N]	Q_a [N]	$\sigma_{B,a}$ [MPa]	N_{exp} [cycles]	$N_{cal,R}$ [cycles]	$\frac{N_{cal,R}}{N_{exp}}$
R1	1200	1100	90	55759	42852	0.77
R2	1200	1100	100	51787	34198	0.66
R3	1000	900	110	59793	51474	0.86
R4	1000	900	125	65614	36043	0.55
R5	650	600	125	52499	75806	1.44
R6	650	600	125	47379	75806	1.60

Table 3. Loading parameters, experimental and estimated fretting fatigue life for specimens No. T1-T7.

TEST No.	P [N]	Q_a [N]	$\sigma_{B,a}$ [MPa]	N_{exp} [cycles]	$N_{cal,T}^{(1)}$ [cycles]	$\frac{N_{cal,T}^{(1)}}{N_{exp}}$	$N_{cal,T}^{(2)}$ [cycles]	$\frac{N_{cal,T}^{(2)}}{N_{exp}}$
T1	1200	1100	90	283522	317811	1.12	385318	1.36
T2	1200	1100	100	191755	238211	1.24	287874	1.50
T3	1000	900	110	238394	404952	1.70	496185	2.08
T4	1000	900	125	196035	259454	1.32	314441	1.60
T5	1000	900	125	214425	259454	1.21	314441	1.47
T6	650	600	125	588006	673885	1.15	837538	1.42
T7	650	600	125	941615	673885	0.72	837538	0.89

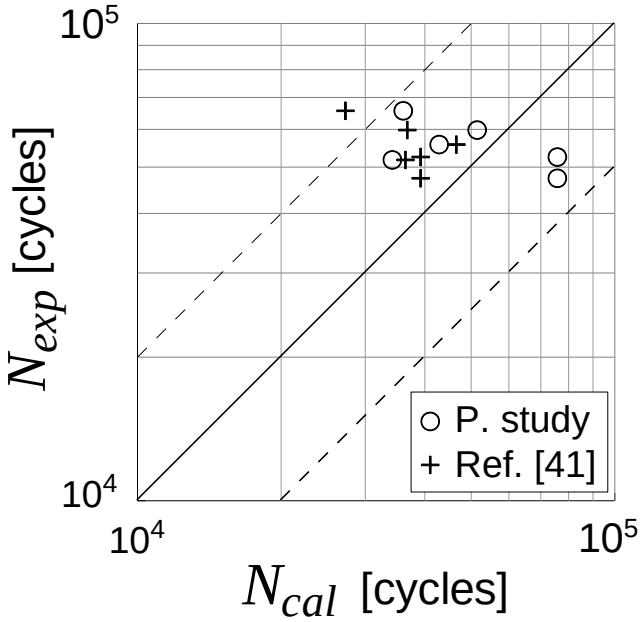

Figure 5. Experimental fatigue life vs estimated fatigue life for each test of the R-series. The results obtained by Vázquez et al.[41] are also reported.

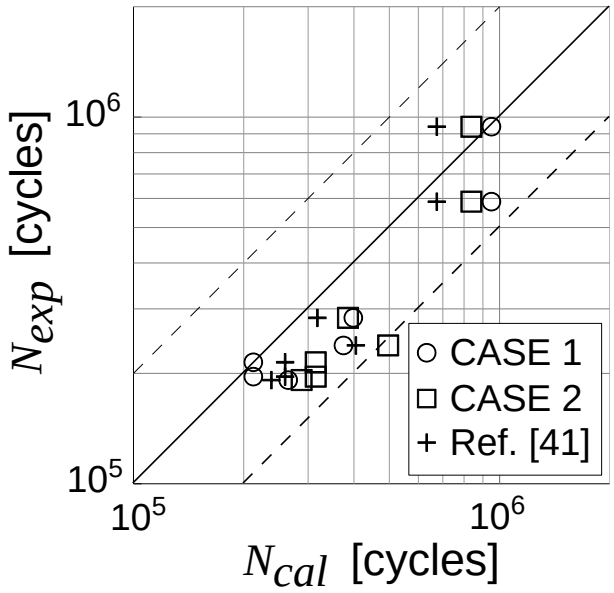

Figure 6. Experimental fatigue life vs estimated fatigue life for each test of the T-series. The results obtained by Vázquez et al.[41] are also reported.

Table 4. Mechanical and fatigue properties of Ti6Al4V alloy[45,47].

MATERIAL	E [GPa]	ν	σ_y [MPa]	σ_u [MPa]	$\sigma_{af,-1}$ [MPa]	m	$\tau_{af,-1}$ [MPa]	m^*	N_0 [cycles]
Ti6Al4V	126	0.32	930	1000	418	9.62	241	9.62	$2\ 10^6$

Table 5. Loading parameters, experimental and estimated fretting fatigue life for specimens No. S1-S11.

TEST No.	P [N]	Q_a [N]	$\sigma_{B,a}$ [MPa]	$\sigma_{B,m}$ [MPa]	N_{exp} [cycles]	$N_{cal,S}$ [cycles]	$\frac{N_{cal,S}}{N_{exp}}$
S1	1335	788	225	275	64258	128608	2.00
S2	1335	1004	225	275	62042	56755	0.91
S3	1335	1010	225	275	60749	54449	0.90
S4	1335	1015	225	275	54295	52598	0.97
S5	1335	762	225	275	3538180	1553865	0.44
S6	1335	775	225	275	2388080	1310277	0.55
S7	1335	985	225	275	153453	258748	1.69
S8	1335	1023	225	275	122579	194035	1.58
S9	1335	1024	225	275	4555510	7845817	1.72
S10	1335	1058	225	275	3986670	5717891	1.43
S11	1335	1097	225	275	2134360	4020383	1.88

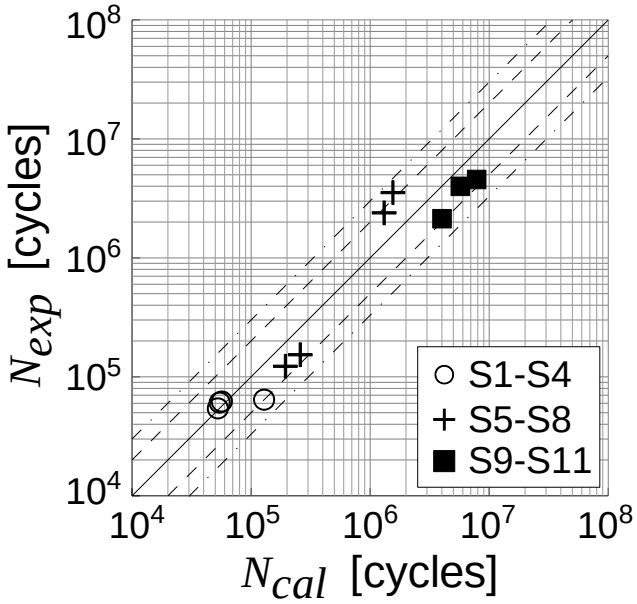

Figure 7. Experimental fatigue life vs estimated fatigue life for each test of the S-series.